Hindawi
Advances in Civil Engineering
Volume 2021, Article ID 6640722, 11 pages
https://doi.org/10.1155/2021/6640722

Research Article

Physical Model Test of Artificial Freezing-Inclined Shaft

Jielong Sun,[1] **Xingzhou Chen**,[2] **Mingming Qiu**,[1] **Xueye Cao**,[1] **and Shaojie Chen**[2]

[1]*School of Architecture and Civil Engineering, Yan'an University, Shaanxi, Yan'an 716000, China*
[2]*School of Architecture and Civil Engineering, Xi'an University of Science and Technology, Xi'an 710054, China*

Correspondence should be addressed to Jielong Sun; sunjielong@126.com

Received 16 December 2020; Revised 15 March 2021; Accepted 19 May 2021; Published 27 May 2021

Academic Editor: Hui Yao

Based on the vertical straight artificial freezing engineering in Northern Shaanxi, a three-dimensional (3D) physical simulation test system was developed, consisting of six parts, which are simulation box, shaft model, loading system, freezing system, external environment simulation system, and data acquisition system. The physical model and actual test results show that the 3D physical simulation test system is reasonable and reliable. The test model results show that the distance from the freezing pipe significantly affects the freezing wall temperature. For the case of four adjacent, two adjacent tangential freezing, and two adjacent axial freezing pipes, the cooling rates were 1.37, 2.79, and 1.96°C/h, respectively. The field measurement showed that the proximity to the freezing pipe increases the cooling rates. The cooling rates of points $1_{k\#}$, $2_{k\#}$, and $3_{k\#}$ were 25.61, 25.32, and 25.35 mm/d, respectively. The increment rates of vertical and horizontal freezing pressures with temperature were 8.78 and 2.97 kPa/°C, respectively. Furthermore, the freezing pressure time fitting formula was given. The calculated results of temperature and freezing pressure are consistent with the measured results, indicating the reasonability and reliability of the 3D physical simulation test scheme of the artificial freezing-inclined shaft in this work.

1. Introduction

Vertical straight-line artificial frozen walls are often used to excavate shafts in areas with large water content, shallow coal seam, and soft soil [1]. However, if the strength of the frozen wall is not enough during the sinking, water gushing and sand flooding are likely to occur, which will pose a threat to the safety of human life and bring about substantial economic losses [2–4]. To ensure that the inclined shaft can safely cross the water-rich soft soil stratum, the formation speed and thickness of the frozen wall must be studied. However, only a few studies of the freezing projects in the inclined shaft can be referenced at present. Such study is an effective and economical method to analyze the distribution law of the freezing temperature and stress in the inclined shaft using a three-dimensional (3D) physical simulation test.

Presently, several studies have investigated the temperature field of frozen walls. Wang and Wei [5] considered the phase change of water in the soil layer and the variation of the freezing temperature with time. The formation of the frozen wall and its temperature field characteristics under oblique conditions were analyzed in detail, using large-scale finite element (FE) software. Yang et al. [6] studied the characteristics of the artificial freezing tunnel test model and prediction of the surrounding rock temperature field. Wang et al. [7] studied the influence of the temperature field of the frozen wall on that of the hydration heat of the outer wall and obtained the basic law of temperature change of the outer and freezing walls during sinking in extra-thick alluvium. Based on the exponential integral function, Li and Xia [8] studied the temperature field of artificially frozen soils and obtained the theoretical expression of the thickness, velocity, and freezing time of the frozen soil curtain. Lü [9] analyzed the temperature variation law thermodynamic-based theory and the phase change law of frozen soils. Cao et al. [10] studied the adaptability of the freezing method under the condition of water-rich sandy pebble stratum and the rationality of the freezing design scheme. Gianpiero et al. [11] studied the artificial ground freezing (AGF) technique to excavate a tunnel below the groundwater table. Li [12] studied the freezing temperature field and thermal

conductivities of two representative soil samples and analyzed the numerical simulation of the freezing temperature with the equivalent thermal conductivity tested, using ANSYS software. Yue et al. [13] simulated the freezing process of artificially frozen soils of Dalian Road tunnel connecting passage with FE analysis (FEA) method and determined the existing varying laws of temperature, displacement, and stress fields. Hu and Zhao [14] studied the precision of the back folding model for the temperature field of AGF. Fan and Yang [15] presented a detailed case study of a cross passage, including the temperature variations in brine, and selected monitoring points around the passage based on field testing results during freezing and frozen wall maintenance. From the above studies mainly about the temperature field distribution of freezing-vertical shaft, the temperature field distribution of freezing-inclined shaft still needs further study.

Wang and Yang [16] established a plane FE model to simulate the whole process of ground frozen-shaft excavation-thawing. Through the sequential coupling of temperature and stress fields, the stress law of the frozen wall during thawing in the surface soil section was obtained. Liu et al. [17] used scale test models to numerically analyze artificial freezing at different temperatures in complicated strata. Vitel et al. [18] modeled the heat transfer between a frozen pipe and the surrounding ground during AGF activities. Zhang et al. [19] studied the transient temperature field of frozen soil with distributed optical fiber. The results showed an inverse correlation and the nonmonotonic correlation between the rate of temperature change of normal frozen soil and its initial water content. Liu and Yan [20] studied the formation and development of frozen walls under the vertical straight-line frozen condition of water-bearing sand stratum and studied the distribution law of frozen wall temperature field in the inclined shaft. Ji et al. [21] presented a model based on 2D heat conduction and calculated the temperature distribution in the frozen wall. Wang et al. [22] used a self-made test device to study the laws of the temperature field and obtain information for predicting the frost heave and numerical simulation of artificially frozen soil. He et al. [23], through numerical simulation analysis and field monitoring data, studied the development law of the temperature field and frozen wall during freezing. Zhang and Yu [24] used the FE method to analyze the formation and temperature distribution of the freezing wall in the artificial freezing method. Hu et al. [25] established AGF temperature field models to study the effect of the soil freezing point on the frozen wall thickness. Shen et al. [26] studied the influence of temperature and moisture content on sandstone thermal conductivity from a case using the AGF method. Kim et al. [27] studied the FE modeling (FEM) and FEA for AGF in egress shafts. Roman et al. [28] studied the AGF of fully saturated soils in a thermal problem. Hou et al. [29] studied the freezing temperature field distribution law of multirow pipes in a large cross-sectional inclined shaft construction. Yao et al. [30] established a calculation model of artificial frozen soil temperature field, based on the support vector machine algorithm, and presented a kernel function suitable for the temperature field. Ren et al. [31] studied the mechanical properties and temperature field of the frozen wall in the water-rich sand layer by combining indoor physical mechanics test, field measurement, and finite element numerical simulation. Sheng and Wei [32] measured the multicircle temperature field of frozen walls and analyzed the problems of the shallow section, deep freezing, cold energy waste, and slow excavation speed of the frozen shaft in the early stage. However, these studies mainly focus on the freezing pressure, temperature field distribution, and the interaction mechanism between freezing wall and shaft wall in freezing-vertical shaft, but the studies on the distribution law of temperature and stress in a freezing-inclined shaft are still rare.

Thus, this work focuses on the freezing engineering of a main inclined shaft in Northern Shaanxi. Based on the characteristics of the sinking freezing-inclined shaft, a set of 3D physical simulation test systems were developed and used for the completed 3D physical simulation test. The results can provide some references for similar projects.

2. Engineering Background

This study is based on the artificial frozen method of a main inclined shaft in Yuan Datan coal mine of Northern Shaanxi. The length of the main inclined shaft, the inclination angle, net section, net width, wall height, and arch height are 1303.3 m, 14°, 16.3 m^2, 5.0 m, 1.25 m, and 2.5 m, respectively. In the upper section, the frozen method is used to sink the shaft. The freezing starting position is 80.215 m from the wellhead, the total inclination length of the frozen section is 377 m, the horizontal length is 365.8 m, and vertical depth of the frozen shaft ranges from 20 to 111.3 m; and the strata of the freezing cross are shown in Table 1.

The water inflow from the main inclined shaft was estimated as 1250 m^3/h from the pumping test. Vertical straight-line artificial frozen method was used to sink the inclined shaft. Five frozen holes with a spacing of 2.35 m from each were made in each row. The thicknesses of the frozen wall on the roof, both sides, and bottom plate were 6.0, 3.0, and 5.0 m, respectively. The layout of frozen holes is shown in Figure 1.

3. Physical Model System

Based on the characteristics of the inclined frozen method, a 3D physical model system for the freezing-inclined shaft was developed. The system consisted of external environment simulation, freezing, model box, and loading; and data acquisition systems are shown in Figures 2–5.

The external environment simulation system in Figure 2 consists of a high- and low-temperature environment laboratory and temperature control system, which can simulate the ambient temperature from 30 to −30°C. The system can keep the laboratory temperature constant and also isolate the heat exchange between the laboratory and external environments to reduce the impact of the external environment on physical test models. The freezing system in Figure 3 consists of a low- and constant-temperature reaction bath and freezing pipe, and the minimum temperature was

Table 1: The strata of the freezing cross.

Stratum	Cumulative depth (m)	Layer thickness (m)	Formation lithology
Q_4^{eol}	7.60	7.60	Silt
Q_3 s	16.83	9.23	Fine sand
Q_3 s	25.30	8.47	Medium sand
Q_3 s	33.60	8.30	Silt
Q_3 s	72.20	38.60	Fine sand
Q_3 s	79.10	6.90	Silt
Q_3 s	97.60	18.50	Fine sand
Q_2 l	98.90	1.30	Loess
J_2 a	110.33	11.43	Sandy mudstone
J_2 a	112.30	1.97	Medium grained sandstone

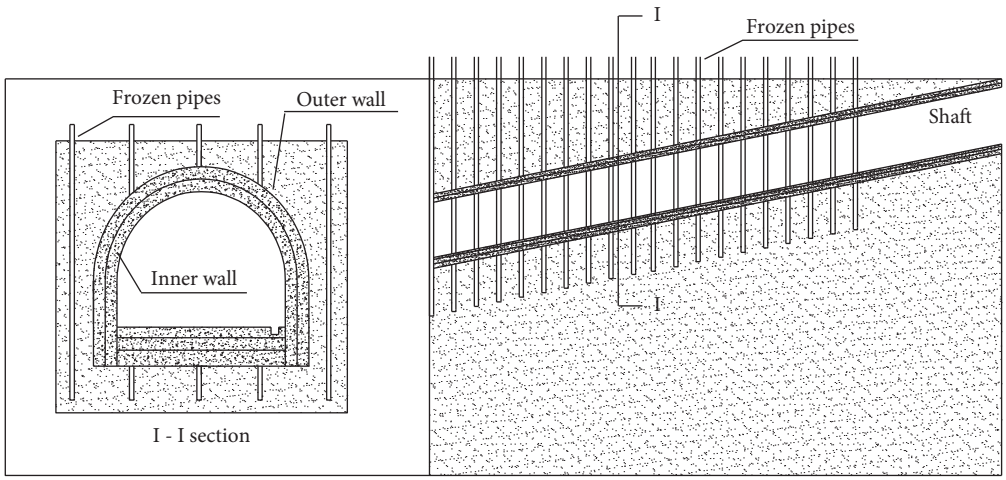

Figure 1: Inclined shaft cross section with frozen pipes.

Figure 2: External environment simulation system. 1: temperature control system, 2: appearance of the incubator, 3: refrigerator, and 4: interior of the incubator.

Figure 3: Freezing system. 1: cold-liquid inlet, 2: cold-liquid outlet, and 3: frozen pipes.

recorded as −30°C. The loading system in Figure 4 consists of a horizontal loading plate and reaction steel channel. The loading plate was placed directly in the box, and the two loading plates were connected by a rubber plate. The reaction steel channel was bolted onto the bottom plate of the box, and the horizontal loading plate was pressed by a jack. The data acquisition system in Figure 5 consists of a static strain gauge, vibrating wire reader, and fiber grating sensor regulator, which can be selected according to different test contents.

4. Physical Simulation Materials and Similarity Criteria

4.1. Physical Simulation Materials. The physical simulation test is an effective method for solving complex problems, and similar materials are the key to such a test. Typical sand was

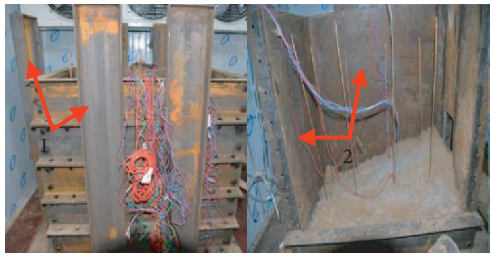

Figure 4: Simulation box and loading system. 1: reaction device; 2: loading plate.

Figure 5: Data acquisition system. 1: static strain gauge, 2: optical sensing interrogator, and 3: vibrating string reader.

used as a similar material in the frozen section of the inclined shaft, and its thermophysical parameters at different temperatures are shown in Table 2 [33].

The density reduction, specific heat capacity reduction, thermal conductivity reduction, and freezing latent heat ratios of water are shown in the following equation:

$$\begin{cases} C_\rho = \dfrac{\rho}{\rho'} = 1, \\ C_C = \dfrac{C}{C'} = 1, \\ C_\lambda = \dfrac{\lambda}{\lambda'} = 1, \\ C_Q = \dfrac{Q}{Q'} = 1, \end{cases} \tag{1}$$

where ρ and ρ' are the densities of the prototype material and physical model, respectively, kg/m^3; C and C' are heat capacities of the prototype material and physical model, respectively, J/(kg·°C); λ and λ' are the thermal conductivities of the prototype material and physical model, respectively, W/(m·°C); Q and Q' are the latent heat values of the freezing water of the prototype material and physical model, respectively, kJ/m^3.

4.2. Geometric Scaling. The model length, width, and height are 1.0, 0.6, and 1.0 m, respectively. Based on Saint-Venant's principle, the soil within 3–5 times of tunnel diameter was selected as the research sample. Also, based on the size of the 3D physical model table, the shaft wall was reversely pushed out and scaled using a geometric ratio of 1 : 50. Thus, the clear width, height, and arc height of the shaft wall model were 100, 25, and 50 mm. In the physical simulation test, a seamless copper pipe with a diameter of 6.35 × 0.7 mm was used for freezing the pipe, and row spacing was 42 × 200 mm.

Table 2: Thermophysical parameters of sand at different temperatures.

Density (kg/m^3)	Temperature (°C)	Heat capacity kJ (kg·°C)	Thermal conductivity W (m·°C)
2190	25	0.998	1.41
	−5	0.667	1.71
	−10	0.849	3.58
	−15	0.553	3.65
	−20	0.546	3.67

4.3. Temperature Scaling. According to the Kosovitch criterion, the temperature scaling can be expressed in the following equation:

$$\begin{cases} \dfrac{Q}{C\rho T} = \dfrac{Q'}{C'\rho' T'}, \\ C_T = \dfrac{T}{T'}, \end{cases} \tag{2}$$

where T and T' are the temperatures of the prototype material and physical model, respectively, °C; C_T is temperature scaling.

Substituting equation (1) into (2) gives $C_T = T/T' = 1$, which means that the temperature of the prototype is consistent with that of the physical simulation test.

4.4. Time Scaling. Based on the Fourier criterion, time scaling can be expressed in the following equation:

$$\begin{cases} \dfrac{\lambda t}{(C\rho R^2)} = \dfrac{\lambda' t'}{(C'\rho' R')}, \\ C_t = \dfrac{t}{t'}, \end{cases} \tag{3}$$

where t and t' are times of the prototype material and physical model, respectively, s; C_t is the time scale. Substituting equations (1) and (2) into equation (3) gives $C_t = 2500$.

5. Test Scheme

5.1. Layout of Temperature Measuring Points. The measuring point arrangement is shown in Figure 6. A total of 21 temperature monitoring points were arranged in the test. The three red measuring points ($1_\#$ to $3_\#$) are affected by four tangential and axially adjacent frozen pipes, which were recorded as monitoring section I. Six black points ($4_\#$ to $9_\#$) were used to monitor the temperature change in the edge zone, which were recorded as monitoring section II. The four

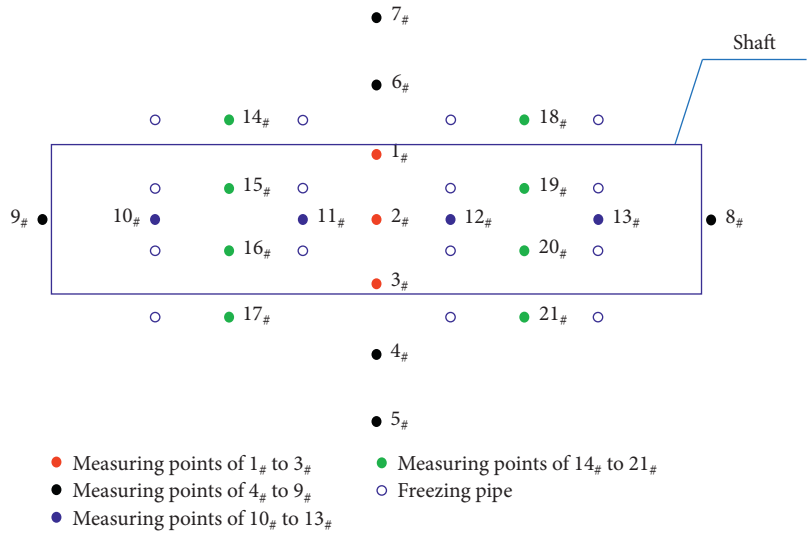

Figure 6: Schematic representation of the temperature measurement points layout.

blue measuring points ($10_{\#}$ to $13_{\#}$) are affected by two adjacent frozen tubes, which are recorded as monitoring section III. The eight green points ($14_{\#}$ to $21_{\#}$) under the influence of two axially adjacent pipes are recorded as monitoring section IV.

5.2. Layout of Pressure Measuring Points. The pressure sensor, which monitors the force change between the shaft and freezing wall during freezing, was mainly arranged on the shaft. The arrangement of the measuring points is shown in Figure 7.

The frozen system will be started after the stabilization of the data of each measuring point. Afterward, the data of each sensor will be recorded. The intersection of the frozen wall surface with different running times during the freezing process is shown in Figure 8.

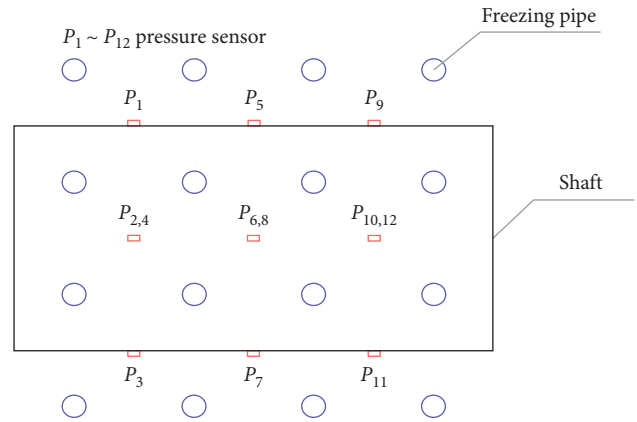

Figure 7: Pressure sensor measuring points.

6. Analysis of Test Results

6.1. Law of Temperature Change. The temperature variation law of each measuring point is shown in Figure 9. The stability of the cold source is one of the important factors ensuring the stable development of the frozen wall. From Figure 9, it took 6 h for the temperature to drop from 27 to 0°C, with the cooling rate at about 4.5°C/h. The cold source temperature reaches −30°C at the 26th hour and the test changes from the active to maintenance-freezing period. The maintenance-freezing temperature was set to −20°C. The cold source temperature began increasing within 36–42 h due to the change of the temperature set value and stabilized at the 56th hour. Afterward, the test entered the maintenance-freezing period. The freezing was stopped at the 120th hour, and the temperature difference of desalinated brine during freezing did not exceed 1°C, which ensured the smooth running of the test.

As shown in Figure 9, points $1_{\#}$, $2_{\#}$, and $3_{\#}$ are affected by four tangential and axially adjacent frozen pipes. During the entire freezing process, the temperature of each measuring point was divided into four stages. The first is a rapid cooling stage, in which the temperature dropped from 27.4 to 0°C at 1.37°C/h, and the lowest temperature was −15.6°C at the 48th hour. At this time, the temperature of each measuring point was higher than −10°C, and the test was changed from the active to the maintenance-freezing period. At the second stage, which is stationary, the temperature of each measuring point stabilized at the 56th hour after a small temperature rise, and the freezing entered the maintenance period. For the third stage, which is the rapid heating stage, the temperature of each measuring point increased rapidly from −12.1 to 0°C in 34 h at 0.38°C/h. At the 210th hour, the temperature of each measuring point culminated to 11.8°C. At the fourth stage, which is stable, the temperature of each measuring point was stable with an average value of 11.1°C. Points $4_{\#}$, $5_{\#}$, $6_{\#}$, $7_{\#}$, $8_{\#}$, and $9_{\#}$ were used to monitor the temperature change of sand at the edge zone of the test model. The distance from point $4_{\#}$ to the shaft axis was equal to that from point $6_{\#}$, while the distance from point $5_{\#}$ to the shaft axis was equal to that from point $7_{\#}$. Points $8_{\#}$ and $9_{\#}$ were located at the ends of the shaft. The cooling speeds of

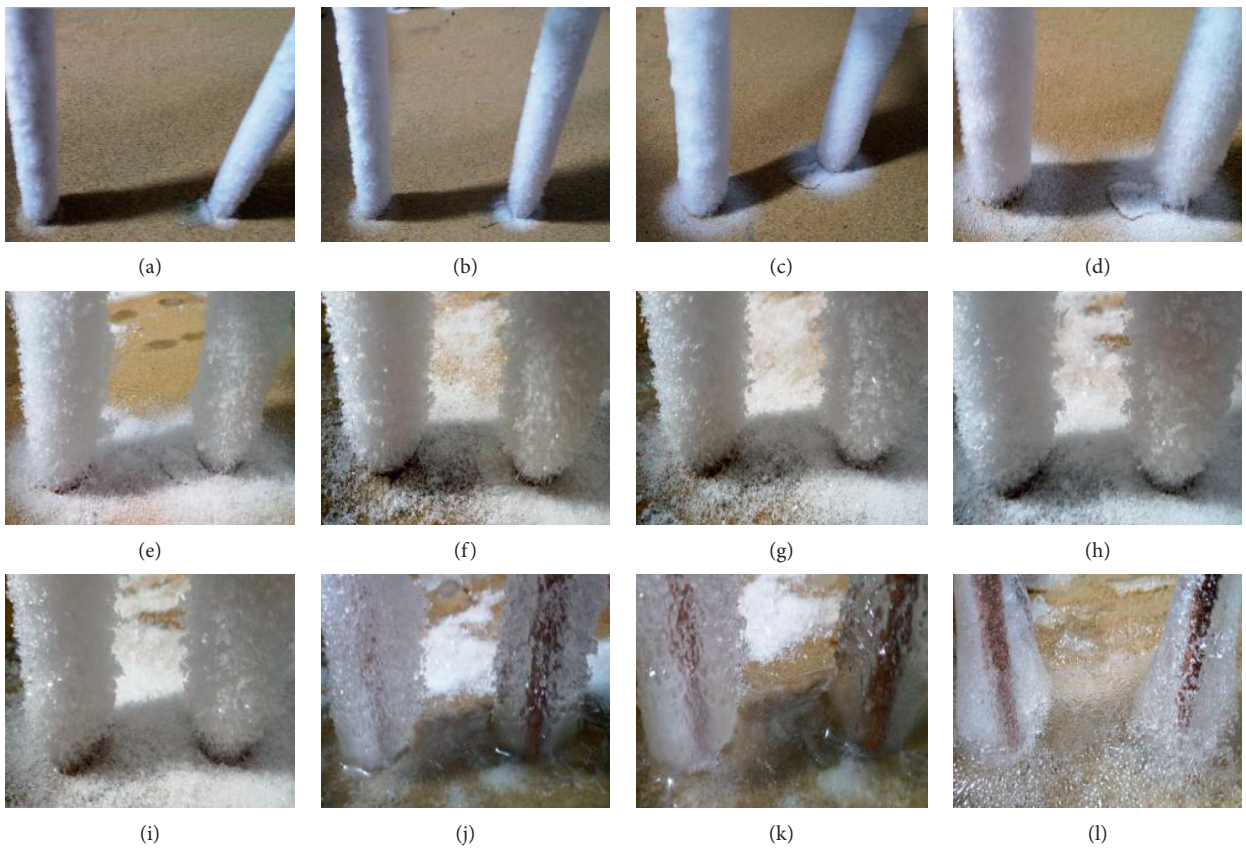

Figure 8: Surface intersection of frozen wall. (a) Boot 2 h. (b) Boot 4 h. (c) Boot 8 h. (d) Boot 10 h. (e) Boot 24 h. (f) Boot 48 h. (g) Boot 72 h. (h) Boot 96 h. (i) Boot 120 h (stop frozen). (j) Shutdown 24 h. (k) Shutdown 48 h. (l) Shutdown 72 h.

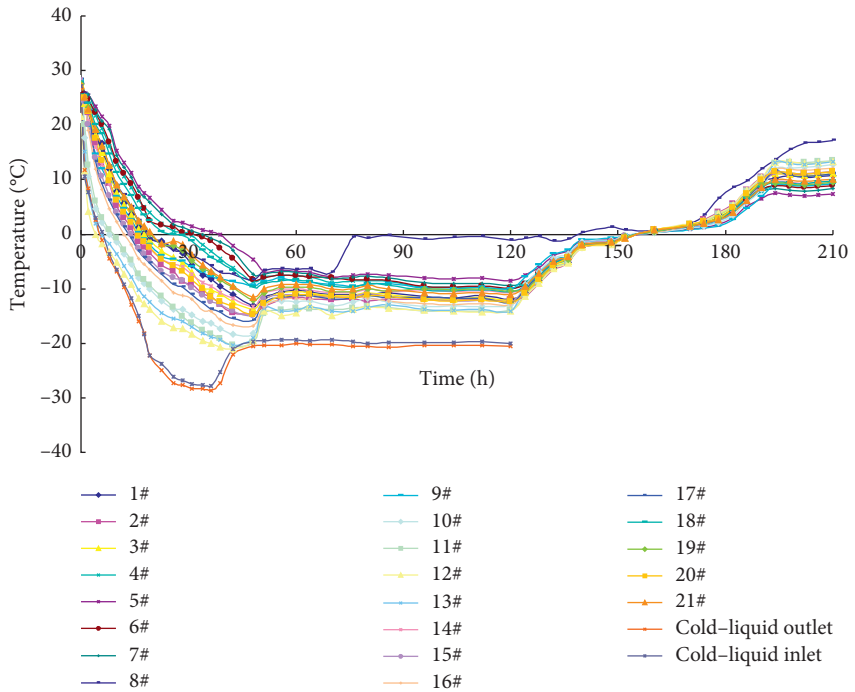

Figure 9: Law of temperature change.

measuring points $4_{\#}$ and $6_{\#}$, $5_{\#}$ and $7_{\#}$, and $8_{\#}$ and $9_{\#}$ were the same, with values of 0.92, 0.82, and 1.57°C/h, respectively. The excavation at the 76th hour exposed measuring point $8_{\#}$ and its temperature was abrupt after 76 h. Points $10_{\#}$, $11_{\#}$, $12_{\#}$, and $13_{\#}$ were used to monitor the temperature change of sand between two adjacent tangential frozen pipes. The temperature variation of each measuring point was the same for points $1_{\#}$–$9_{\#}$ during freezing, and both had rapid cooling, stationary, rapid heating, and stable stages. The temperature variation of each measuring point was the same and the cooling rate was about 2.79°C/h. During the test change from the active to the maintenance-freezing period, the temperatures of points $10_{\#}$–$13_{\#}$ were smaller than those of points $4_{\#}$–$9_{\#}$, due to the proximity of points $10_{\#}$–$13_{\#}$ to the freezing pipe. Thus, a larger cooling capacity was obtained. Measuring points $14_{\#}$, $15_{\#}$, $16_{\#}$, $17_{\#}$, $18_{\#}$, $19_{\#}$, $20_{\#}$, and $21_{\#}$ monitored the temperature change of sand between two adjacent frozen pipes in the axial direction. The temperature variation of each measuring point was the same for points $4_{\#}$–$13_{\#}$ during freezing, and the cooling rate was about 1.96°C/h.

In summary, the cooling rate of points $10_{\#}$–$13_{\#}$ was the fastest, followed by that of points $14_{\#}$–$21_{\#}$ and then points $1_{\#}$–$3_{\#}$. The cooling rate of points $10_{\#}$–$13_{\#}$ was the slowest because of the smaller distance from points $10_{\#}$–$13_{\#}$ and $14_{\#}$–$21_{\#}$ to the cold source compared to that from points $14_{\#}$–$21_{\#}$ and points $1_{\#}$–$3_{\#}$, respectively. Moreover, the distance from points $1_{\#}$–$3_{\#}$ to the cold source was smaller than that from points $4_{\#}$–$9_{\#}$.

The heat conduction process of frozen wall is shown in Figure 10; r_1 is the radius of freezing pipes, r_2 is the radius of frozen wall, r is the radius of a certain point in the frozen wall, and dr is the radius of the micro unit. T_1 and T_2 are temperatures of cold source and outer boundary of frozen wall. According to Fourier heat conduction law, the heat transfer rate of frozen wall is shown in the following equation:

$$Q = -\lambda 2\pi L \frac{dT}{dr}, \tag{4}$$

where L is freezing pipe length and λ represents the thermal conductivities.

Equation (4) shows that heat transfer rate is proportional to the temperature difference and inversely proportional to the distance. In the freezing process, the time is equal and the temperature difference is constant, so the heat transfer rate is related to the distance. The larger the distance, the smaller the heat transfer rate and the slower the cooling rate.

Equation (4) and physical simulation test results show that the distance from the cold source significantly influences the cooling rate.

6.2. Distribution and Variation of Freezing Pressure. The distribution and variation of freezing pressure are shown in Figure 11. Points $2^{\#}$, $4^{\#}$, $6^{\#}$, $8^{\#}$, $10^{\#}$, and $12^{\#}$ monitor the vertical freezing pressure. The maximum vertical freezing pressure is 353.86 kPa at the 48th hour and the rate of increment is 7.32 kPa/h. From Figure 9, the freezing wall temperature is

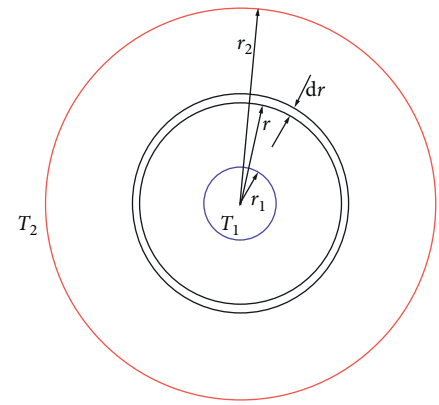

Figure 10: Heat conduction of frozen wall.

lowest at the 48th hour. Also, the minimum and initial temperatures are −13.2 and 27.1°C, respectively; thus the rate of increment of the vertical freezing pressure with temperature is 8.78 kPa/°C. Points $1^{\#}$, $3^{\#}$, $5^{\#}$, $7^{\#}$, $9^{\#}$, and $11^{\#}$ monitor the horizontal freezing pressure. Furthermore, the maximum vertical freezing pressure is 119.55 kPa at the 48th hour with an increment rate of 2.49 kPa/h and the increment rate of the horizontal freezing pressure with temperature is 2.97 kPa/°C. Besides, the vertical freezing pressure is 2.96 times the horizontal freezing pressure.

As shown in Figures 9 and 11, the temperature change significantly influences the freezing pressure. During the active-freezing period, the temperature decreases rapidly, while the freezing pressure increases rapidly. The freezing pressure tends to stabilize at the 56th hour because of the temperature stabilization of each measuring point. Freezing stopped at the 120th hour when the temperature of the freezing wall increased and the freezing pressure began to decrease.

7. Field Measurement and Rationality Verification of the Test Model

To verify the rationality of the 3D physical simulation test scheme proposed in this study, field measurements of freezing wall temperature and pressure were carried out. The temperature and freezing pressure monitoring points are shown in Figure 12.

7.1. Analysis of Field Measurement Results

7.1.1. Temperature. The measured results of the freezing wall temperature are shown in Figure 13. The cooling rate of sand during the active-freezing period is approximately linear with time, and the temperature difference among the three temperature measuring points is small. During the active-freezing period, the cooling rate of $1_{k\#}$ is the fastest because of its proximity to the freezing pipes, while those of $2_{k\#}$ and $3_{k\#}$ are equal. When the freezing period enters the maintenance period, the temperature of point $1_{k\#}$ is lower than those of points $2_{k\#}$ and $3_{k\#}$, due to its proximity to the freezing pipes. The sand showed a faster cooling rate at this

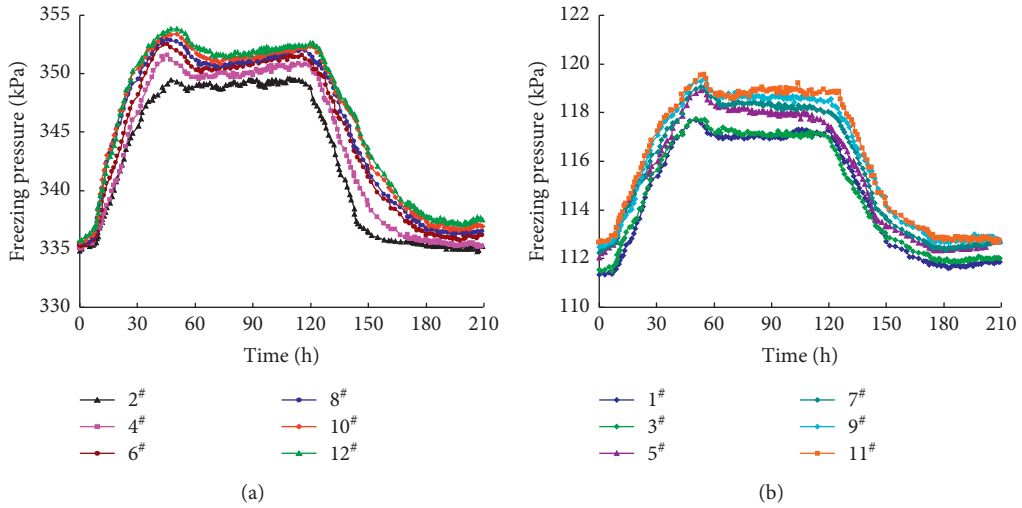

Figure 11: Low freezing pressure change. (a) Vertical freezing pressure. (b) Horizontal freezing pressure.

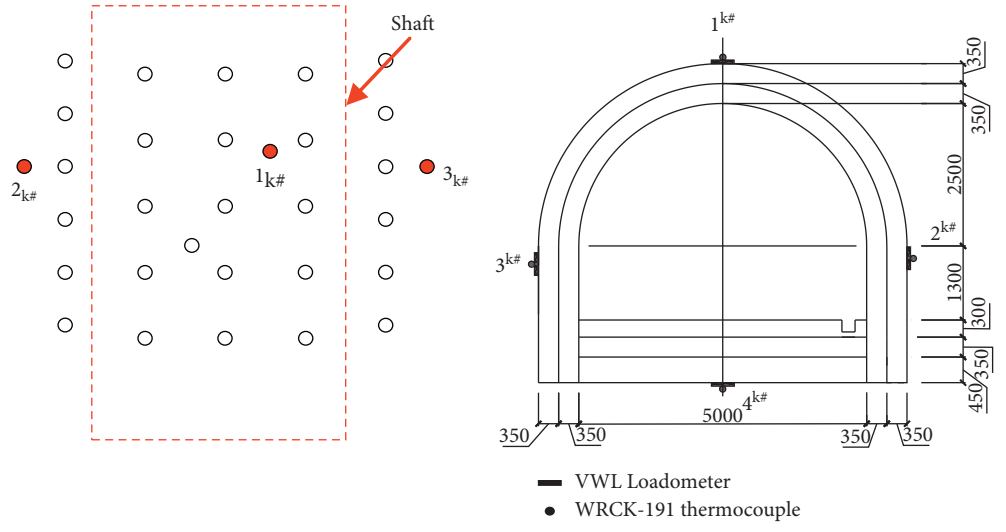

Figure 12: On-site monitoring points. (a) Temperature monitoring points. (b) Freezing pressure monitoring points.

stage. The cooling rates of points $1_{k\#}$, $2_{k\#}$, and $3_{k\#}$ are 25.61, 25.32, and 25.35 mm/d, respectively.

7.1.2. Freezing Pressure. The measured results of pressure and temperature are shown in Figure 14. Due to the large amount of hydration heat produced by the concrete pouring of the shaft lining, the local temperature field of the freezing wall increases to a maximum temperature of 16.7°C. When the hydration heat of concrete dissipates, the frozen wall begins to refreeze on the 6th day, and the freezing pressure increases. The freezing stops on the 17th day and the frozen wall begins to thaw. Thus, the supporting effect of the frozen wall decreases, and the surrounding water and soil pressure are mainly borne by the shaft. The sensor pressure then culminates to 370.76 kPa.

7.2. Comparative Analysis

7.2.1. Temperature. Measuring points $11_{\#}$, $4_{\#}$, and $6_{\#}$ correspond to measuring points $1_{k\#}$, $2_{k\#}$, and $3_{k\#}$, respectively. Based on the time scale, the inverse of the actual temperature of the measuring point corresponding to the temperature of each measuring point in the physical simulation test was calculated and plotted (Figure 15). Figure 15 shows that, due to certain differences between the on-site and indoor physical simulation tests, the physical simulation temperature could not perfectly match with that of the on-site measured data, but the cooling laws of all measuring points were equal, which indicates that the 3D physical simulation test scheme of the artificial freezing-inclined shaft in this study is feasible and better reflects the general law of artificial freezing-inclined shaft cooling.

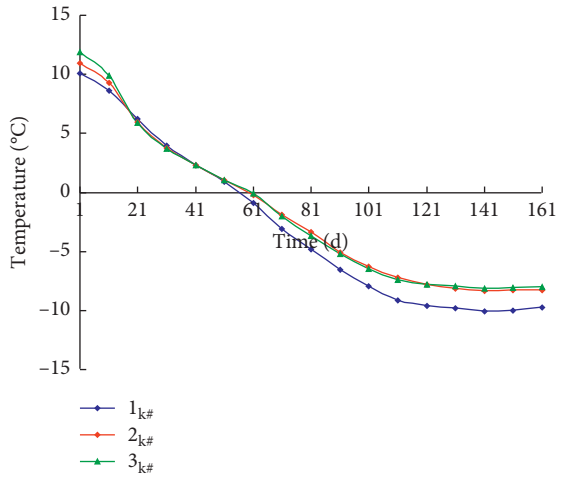

Figure 13: Measured temperature.

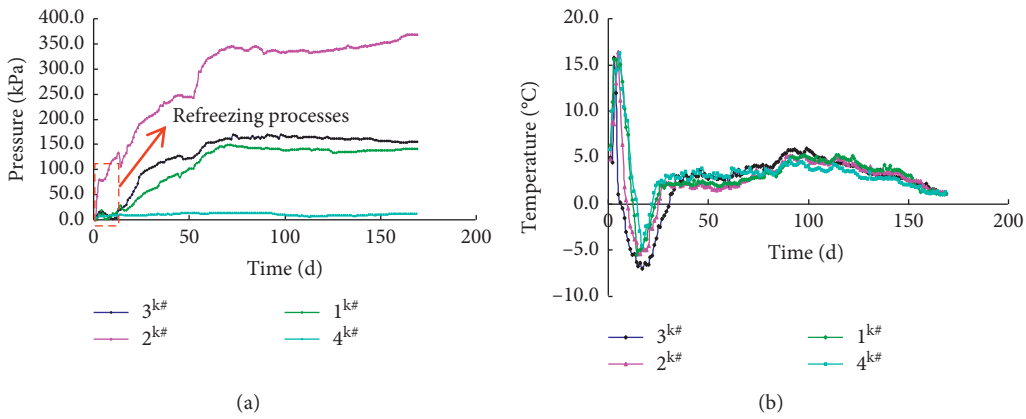

Figure 14: Measured (a) pressure and (b) temperature.

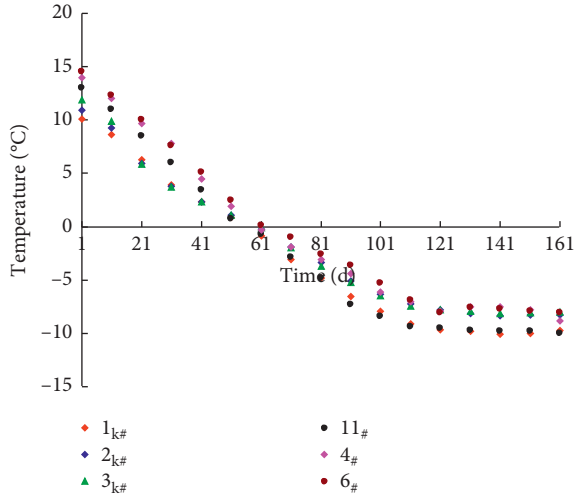

Figure 15: Comparison curve of test and measured temperatures.

7.2.2. Freezing Pressure. During the active-freezing period, the relationship between the freezing pressure and temperature can be expressed by a quadratic polynomial, as shown in the following equation:

$$P = p_1 T^2 - p_2 T + p_3, \tag{5}$$

where p_1, p_2, and p_3 are fitting coefficients.

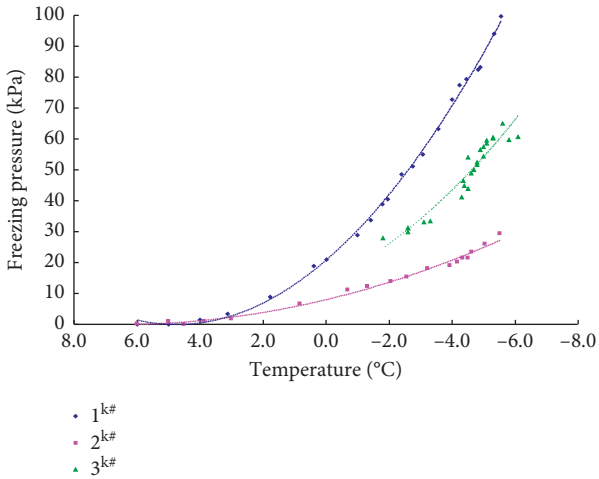

Figure 16: Calculated and measured temperature-freezing pressure curves.

Table 3: Fitting coefficients.

Fitting coefficients	$1_{k\#}$	$2_{k\#}$	$3_{k\#}$
p_1	0.924	0.186	0.679
p_2	−8.777	−2.452	−4.576
p_3	20.787	8.005	14.313

The monitoring instruments were embedded after excavation in the actual project because those of the test model were embedded in advance. This disparity resulted in different freezing pressure changes for both scenarios. However, after the concrete hydration heat dissipated, the freezing wall began freezing. During such a process, the relationship between the temperature change and freezing pressure is expected to satisfy equation (4), which is shown in Figure 16. The fitting coefficients are presented in Table 3.

It can be seen from Figure 16 that the calculated results of temperature and freezing pressure are consistent with the measured results, which further indicates that the 3D physical simulation test scheme of the artificial freezing-inclined shaft in this work is reasonable and reliable.

8. Conclusions

In this study, a 3D physical simulation test system was developed to test the vertical straight-line artificial freezing-inclined shaft and conduct field measurements of the freezing wall temperature and pressure. The results of this study can be summarized as follows:

(1) A 3D physical simulation test system was developed; the comparison between the model and the actual test results showed the reasonability and reliability of the 3D physical simulation test system.

(2) Theoretical analysis, test model, and field measurement results show that the distance from the cold source significantly influences the cooling rate, and the proximity to the frozen pipe increases the cooling speed of the freezing wall.

(3) The temperature change significantly affects the freezing pressure; the relationship between the freezing pressure and temperature can be expressed by a quadratic polynomial. Furthermore, the freezing pressure time fitting formula was given, and the calculated results of temperature and freezing pressure are consistent with the measured results.

Data Availability

All data generated or analyzed during this study are included within this article.

Conflicts of Interest

The authors declare that there are no conflicts of interest regarding the publication of this paper.

Acknowledgments

This study was supported by the National Natural Science Foundation of China (no. 51979218), Joint Fund Project of the National Natural Science Foundation of China (no. U1965107), Natural Science Foundation of Shaanxi (nos. 2019JQ-832 and 2018JM5118), General Special Scientific Research Program of Shaanxi Provincial Department of Education (no. 20JK0985), and Doctoral Research Start-Up Project of Yan'an University (no. YDBK2018-25).

References

[1] Q.-B. Meng, L.-J. Han, R.-J. Shi et al., "Study and application of construction technology for inclined shafts penetrating drift sand strata in coal mine," *Chinese Journal of Geotechnical Engineering*, vol. 37, no. 5, pp. 900–910, 2015.

[2] G. Shao-Hua, L. Yan, L. Zhen-Zhong et al., "Progress in research on reliability of inclined shaft frozen wall," *Coal Technology*, vol. 34, no. 10, pp. 49–51, 2015.

[3] J.-L. Fan, W. Yuan-Chao, and W. Wang, "Construction technology of freeze sinking method in inclined shaft soil layer," *Coal Science and Technology*, vol. 41, no. 9, pp. 143–150, 2013.

[4] X.-.E. Chen and D. Chang-Long, "Freezing construction technology of mine inclined shaft in Mataihao mine," *Coal Science and Technology*, vol. 37, no. 11, pp. 21–23, 2009.

[5] R.-H. Wang and W. Wei, "Analysis for features of the freezing temperature field under deflective pipes," *Chinese Journal of Geotechnical Engineering*, vol. 25, no. 6, pp. 658–661, 2003.

[6] L. Yang, Z. Yao, and Z. Jiang, "Artificial freezing tunnel model test and prediction of surrounding rock temperature field," *Sichuan Building Materials*, vol. 44, no. 8, pp. 66-67+69, 2018.

[7] Y.-S. Wang, H. Jia-Hui, W.-H. Y. et al., "Temperature measurement of outer shaft wall during freezing sinking in deep alluvium," *Journal of China University of Mining & Technology*, vol. 35, no. 4, pp. 468–472, 2006.

[8] F.-Z. Li and M.-P. Xia, "Study on analytical solution of temperature field of artificial frozen soil by exponent-integral function," *Journal of Southeast University (Natural Science Edition)*, vol. 4, pp. 469–473, 2004.

[9] S. Lü, "Numerical analysis of temperature field on artificial frozen wall," *Natural Science Journal of Harbin Normal University*, vol. 25, no. 3, pp. 43–45, 2009.

[10] J. Cao, W. Wang, P. Zheng et al., "Analysis of artificial freezing temperature field for connected adit in water-rich sandy pebble stratum," *Railway Engineering*, vol. 59, no. 12, pp. 55–59, 2019.

[11] R. Gianpiero, A. Corbo, F. Cavuoto et al., "Artificial ground freezing to excavate a tunnel in sandy soil. measurements and back analysis," *Tunnelling and Underground Space Technology Incorporating Trenchless Technology Research*, vol. 50, 2015.

[12] Y. Li, *Experimental Study on Thermal Conductivity of Artificial Frozen Clay and Develop Rules of Multi-freezing-Tube Temperature Field*, Anhui University of Science and Technology, Huainan, China, 2015.

[13] F. T. Yue, S. G. Lv, R. J. Shi et al., "Numerical analysis and spot-survey study of horizontal artificial ground freezing in tunnel connecting passage construction," *Applied Mechanics and Materials*, vol. 3843, 2015.

[14] X. Hu and J. Zhao, "Research on precision of Bakholdin model for temperature field of artificial ground freezing," *Chinese Journal of Underground Space and Engineering*, vol. 6, no. 1, pp. 96–101, 2010.

[15] W. Fan and P. Yang, "Ground temperature characteristics during artificial freezing around a subway cross passage," *Transportation Geotechnics*, vol. 20, 2019.

[16] Y. Wang and W.-H. Yang, "Study on mechanical law of freezing inclined shaft lining in topsoil during frozen wall thawing," *Coal Science and Technology*, vol. 44, no. 5, pp. 133–139, 2016.

[17] B. Liu, Y. Chen, D. Li et al., "Scale model tests and numerical analysis of artificial freezing at different temperatures in complicated strata," *Chinese Journal of Rock Mechanics and Engineering*, vol. 32, no. Z2, pp. 3328–3336, 2013.

[18] M. Vitel, A. Rouabhi, M. Tijani, and F. Guérin, "Mode ling heat transfer between a freeze pipe and the surrounding ground during artificial ground freezing activities," *Computers and Geotechnics*, vol. 63, 2015.

[19] W. Zhang, B. Shi, W.-B. Suo et al., "Monitoring and application of distributed optical fiber sensors in transient temperature field of frozen soil," *Chinese Journal of Geotechnical Engineering*, vol. 29, no. 5, pp. 723–728, 2007.

[20] B. Liu and L. Yan, "Study on temperature field distribution law of freezing wall for inclined shaft," *Coal Science and Technology*, vol. 40, no. 12, pp. 4–7, 2012.

[21] Z.-Q. Ji, X.-Y. Xu, and L.-L. Yu, *Study on the Influence of Artificial Frozen Soil Layer to the Temperature Field and Displacement Field of the Frozen Wall*, pp. 98-99, State Key Laboratory of Frozen Soil Engineering, Lanzhou, China, 2006.

[22] W. Wang, J. Wang, X. Jing et al., "Experimental study of temperature field in course of artificial freeang," *Journal of China University of Mining & Technology*, vol. 33, no. 4, pp. 388–391+405, 2004.

[23] X.-N. He, D.-B. Du, X. Zhou et al., "Numerical analysis and field monitoring on the frozen temperature field of vertical hole in the inclined shaft," *Mining Research and Development*, vol. 37, no. 11, pp. 94–98, 2017.

[24] Y. Zhang and S. Yu, "Using finite element method to analyze the formation and temperature distribution of the freezing-wall in the artificial freezing method," *Journal of Engineering Thermophysics*, vol. 5, no. 2, pp. 175–181, 1984.

[25] X. D.. Hu, F. Huang, and N. Bai, "Models of artificial frozen temperature field considering soil freezing point," *Journal of China University of Mining & Technology*, vol. 37, no. 4, pp. 550–555, 2008.

[26] Y.-J. Shen, Y.-Z. Wang, X.-D. Zhao et al., "The influence of temperature and moisture content on sandstone thermal conductivity from a case using the artificial ground freezing (AGF) method," *Cold Regions Science and Technology*, vol. 155, 2018.

[27] Y. S. Kim, J.-M. Kang, J. Lee et al., "Finite element mode ling and analysis for artificial ground freezing in egress shafts," *KSCE Journal of Civil Engineering*, vol. 16, no. 6, 2012.

[28] L. Roman, A. Amon, and H. Lagger, "Artificial ground freezing of fully saturated soil: thermal problem," *Journal of Engineering Mechanics*, vol. 131, no. 2, 2005.

[29] Y.-B. Hou, J. Jin-Fend, Y.-X. Zhao et al., "Simulation study on freezing temperature field with multi row freezing tubes in construction of large cross section mine inclined shaft," *Coal Engineering*, vol. 1, no. 12, pp. 77–80, 2012.

[30] Z.-M. Yao, L. Zheng-Fei, and J.-H. Chen, "Study on support vector machine method prediction of artificial ground freezing temperature field," *Coal Engineering*, vol. 9, pp. 87–89, 2012.

[31] J.-X. Ren, J.-L. Sun, K. Zhang et al., "Study of mechanical properties and temperature field of inclined frozen wall in water-rich sand stratum," *Rock and Soil Mechanics*, vol. 38, no. 5, pp. 1405–1412, 2017.

[32] T. B.. Sheng and S.-Y.. Wei, "Measurement and engineering application of temperature field multiple-ring hole frozen wall in extra-thick clay strata," *Chinese Journal of Geotechnical Engineering*, vol. 34, no. 8, pp. 1516–1521, 2012.

[33] J. Sun, J. Ren, S. Li et al., "Experimental study on the physical mechanics characteristics of sand under different frozen temperatures," *Journal of Yanan University (Natural Science Edition)*, vol. 38, no. 3, pp. 38–44, 2019.